

Heterogeneous Charge Mobility in Individual Conjugated Polyelectrolyte Nanoparticles Revealed by Two-Color Single Particle Spectroelectrochemistry Studies

Robert Pierre Godin, Rodrigo E Palacios, and Gonzalo Cosa

J. Phys. Chem. C, **Just Accepted Manuscript** • DOI: 10.1021/acs.jpcc.5b03491 • Publication Date (Web): 19 May 2015

Downloaded from <http://pubs.acs.org> on June 1, 2015

Just Accepted

“Just Accepted” manuscripts have been peer-reviewed and accepted for publication. They are posted online prior to technical editing, formatting for publication and author proofing. The American Chemical Society provides “Just Accepted” as a free service to the research community to expedite the dissemination of scientific material as soon as possible after acceptance. “Just Accepted” manuscripts appear in full in PDF format accompanied by an HTML abstract. “Just Accepted” manuscripts have been fully peer reviewed, but should not be considered the official version of record. They are accessible to all readers and citable by the Digital Object Identifier (DOI®). “Just Accepted” is an optional service offered to authors. Therefore, the “Just Accepted” Web site may not include all articles that will be published in the journal. After a manuscript is technically edited and formatted, it will be removed from the “Just Accepted” Web site and published as an ASAP article. Note that technical editing may introduce minor changes to the manuscript text and/or graphics which could affect content, and all legal disclaimers and ethical guidelines that apply to the journal pertain. ACS cannot be held responsible for errors or consequences arising from the use of information contained in these “Just Accepted” manuscripts.

1
2
3
4
5
6
7
8
9
10
11
12
13
14
15
16
17
18
19
20
21
22
23
24
25
26
27
28
29
30
31
32
33
34
35
36
37
38
39
40
41
42
43
44
45
46
47
48
49
50
51
52
53
54
55
56
57
58
59
60

Heterogeneous Charge Mobility in Individual Conjugated Polyelectrolyte Nanoparticles Revealed by Two-Color Single Particle Spectroelectrochemistry Studies

Robert Godin¹, Rodrigo Palacios² and Gonzalo Cosa^{1,}*

¹Department of Chemistry and Center for Self-Assembled Chemical Structures
(CSACS/CRMAA), McGill University, 801 Sherbrooke Street West, Montreal, QC, H3A 0B8,
Canada. ²Departamento de Química, Facultad de Ciencias Exactas Físico-Químicas y Naturales,
Universidad Nacional de Río Cuarto, Río Cuarto, Córdoba, Argentina

*email:gonzalo.cosa@mcgill.ca

1
2
3
4 ABSTRACT
5
6
7

8 The optoelectronic properties of conjugated polymers and conjugated polyelectrolytes (CPEs)
9 depend on their chain conformation and packing. Correlations between emission color, charge
10 mobility and extent of aggregation in these materials have been previously established from bulk
11 studies. Here we describe the preparation of stable nanoparticle suspensions of the CPE poly[5-
12 methoxy-2-(3-sulfopropoxy)-1,4-phenylenevinylene (MPS-PPV) where changes in the solvent
13 composition enable tuning their emission spectra and quantum yield. Employing a newly
14 developed color-sensitive single-molecule spectroelectrochemistry (SMS-EC) technique, the
15 effect of chain conformation on the optoelectronic properties of MPS-PPV nanoparticles is
16 monitored at the single particle level. Within a single particle the photoluminescence and redox
17 response is chromatically-correlated reflecting on the differing contributions that coiled and
18 deaggregated vs. extended and packed segments have on their optoelectronic properties. We also
19 observe a heterogeneous response among nanoparticles to externally applied electrochemical
20 potentials which further correlates with their emission color (chain packing). We rationalize our
21 observations on differential charge injection, energy and charge transport and ion migration as a
22 consequence of chain conformation, packing effects, and the presence of electrochemically
23 reducible quenching sites. Our work provides a way to unravel the intrinsic heterogeneity of CPE
24 materials to better understand the relationship between chain conformation and optoelectronic
25 properties.
26
27
28
29
30
31
32
33
34
35
36
37
38
39
40
41
42
43
44
45
46
47
48
49
50
51
52
53
54
55
56
57
58
59
60

1
2
3 INTRODUCTION
4
5
6

7 Conjugated polymers and conjugated polyelectrolytes (CPEs)¹ have become customary
8 building blocks for optoelectronic devices such as LEDs, thin-film transistors, chemical sensors,
9 and photovoltaics.²⁻⁸ Their increasing importance in the manufacturing industry arises both from
10 their ease of processability and tunable electronic and optical properties. These properties are
11 intimately related to the conformation of individual chains along the polymer backbone and to
12 the distance between chains.⁹⁻¹⁴ In this context, increased charge carrier mobilities, reduced
13 emission quantum yield, red-shifted emission spectrum, and increased exciton transport
14 properties have been observed experimentally as a result of the increase of conjugation length
15 caused by extension of the polymer backbone as well as by the formation of interchain species.¹⁵⁻

16
17
18
19
20
21
22
23
24
25
26
27
28
29
30
31
32
33
34
35
36
37
38
39
40
41
42
43
44
45
46
47
48
49
50
51
52
53
54
55
56
57
58
59
60

21
22
23
24
25
26
27
28
29
30
31 Given the amphiphilic nature of CPEs (hydrophobic backbone with π -delocalized electronic
32 structure and repeat units that bear pendant substituents with ionic functionalities)¹ their chain
33 conformation and extent of aggregation in solution may be tuned upon careful solvent choice.²²⁻
34
35
36
37
38
39
40
41
42
43
44
45
46
47
48
49
50
51
52
53
54
55
56
57
58
59
60
25 CPEs provide in this regard unique systems to explore how the interplay of chain
conformation and aggregation affect electronic and optical properties at the nanoscale.

Here we show that adjusting the water content in water/tetrahydrofuran (H₂O/THF) and
water/acetonitrile (H₂O/MeCN) mixtures enables controlling the chain conformation and
aggregation of the conjugated polyelectrolyte poly[5-methoxy-2-(3-sulfopropoxy)-1,4-
phenylenevinylene] (MPS-PPV, see Figure 1). Conjugated polyelectrolyte nanoparticles (NPs)
with emission spectra peaking in the range from ca. 620 nm to 545 nm and with up to 46-fold

1
2
3 increase in relative emission intensity are readily obtained upon careful selection of the solution
4
5 conditions.
6
7

8 We also show that the effect of chain conformation on the optical and electronic properties of
9
10 MPS-PPV can be monitored at the single nanoparticle level with the aid of a novel color-
11
12 sensitive single-molecule spectroelectrochemistry (SMS-EC) technique. This technique enabled
13
14 recording the distribution of the potentials required to inject charges (both from the ground state
15
16 and photoexcited states) for individual CPE NPs, offering new information on the heterogeneity
17
18 of the redox process of CPEs at the molecular level. The simultaneous monitoring of the red
19
20 (extended/aggregated polymer backbone) and green (coiled and deaggregated backbone)
21
22 emission components as a function of applied bias in an electrochemical cell configuration
23
24 allowed us to unearth the interplay between charge injection (thermal and photoinduced), energy
25
26 transfer and photoluminescence in individual MPS-PPV NPs and correlate them to CPE
27
28 conformation.²⁶ We demonstrate that NPs of MPS-PPV display differing emissive behavior
29
30 when subjected to an externally applied electrochemical bias. This is manifested both in the
31
32 response speed and modulation amplitude exhibited between different nanoparticles. Within a
33
34 single particle the photoluminescence response is also chromatically-correlated reflecting on the
35
36 differing contributions that coiled and deaggregated vs. extended and packed segments have on
37
38 the optoelectronic properties.
39
40
41
42
43
44

45 Our studies provide a method that distinguishes between individual MPS-PPV NPs with lower
46
47 or higher charge mobility, caused by chain packing effects for example, and thus make it
48
49 possible to evaluate the effectiveness of various approaches aimed at modifying chain
50
51 conformation for specific applications. Our work provides a way to unravel the intrinsic
52
53
54
55
56
57
58
59
60

1
2
3 heterogeneity of CPE materials to better understand the relationship between chain conformation
4 and optoelectronic properties.
5
6
7
8
9

10 EXPERIMENTAL SECTION

11 **Preparation of MPS-PPV solution in H₂O/organic solvent for ensemble measurements.**

12
13 An initial MPS-PPV stock solution (0.25% w/w in H₂O, 9.5 mM in polymer repeat units) was
14
15 centrifuged for 5 min at 5000 rpm on a benchtop centrifuge (accuSPINTM micro, Fisher
16
17 Scientific) to precipitate large aggregates. In order to prepare the various H₂O/organic solvent
18
19 dispersions, 10 μ L aliquots of the supernatant were brought to a final desired H₂O volume before
20
21 adding to the organic solvent in order to complete 2 mL of H₂O:organic solution with the desired
22
23 % v/v H₂O content. To ensure reproducibility, the aqueous MPS-PPV solution thus obtained was
24
25 diluted at most 10x in the water-miscible solvents THF or MeCN by rapid injection, and next the
26
27 resulting solution was added to the remaining organic solvent to complete 2 mL. For H₂O
28
29 volumes > 200 μ L, a single injection was performed into the organic solvent to yield a final
30
31 volume of 2 mL. The MPS-PPV stock was thus diluted 200-fold in all ensemble experiments
32
33 yielding a final polymer repeat unit concentration of 48 μ M.
34
35
36
37
38
39
40

41 **Ensemble spectroscopy.** Fluorescence measurements were performed on a PTI Quantamaster
42
43 40 fluorimeter at 25°C with excitation at 450 nm. UV-VIS spectra were obtained at room
44
45 temperature (23 \pm 1 °C) on a Hitachi U-2800 spectrophotometer. DLS measurements were
46
47 performed on a Brookhaven Instruments NanoBrook 90Plus at 90° detection angle, 25°C with
48
49 nominally 640 nm laser light.
50
51
52

53 **SEM imaging.** Coverslips were cleaned immersing them for 1h in a piranha solution (30%
54
55 H₂O₂ and H₂SO₄ 1:3 v:v). They were next thoroughly rinsed with H₂O and EtOH. MPS-PPV NPs
56
57
58
59
60

1
2
3 (0.5% v/v H₂O content) were spin-coated by dropping 40 μL of solution on the clean coverslips
4
5 rotating at 3000 rpm. The spinning was then slowed to 2000 rpm and kept for 50 s afterwards. A
6
7 thin gold coating (~ 10 nm) was then argon-sputtered in a vacuum environment to give sufficient
8
9 sample conductivity. The SEM images were acquired on a FEI Inspect F-50 FEG-SEM operating
10
11 at 10-20 kV in backscatter detection mode.
12
13

14
15 **Single molecule spectroelectrochemistry.** MPS-PPV NPs (0.5% v/v H₂O content in THF)
16
17 were spin-coated by dropping 40 μL of solution on a clean ITO-coated coverslip (Evaporated
18
19 Coatings Inc., 50 Ω/□; cleaned by 20 minutes sequential sonication in acetone, trichloroethylene
20
21 and methanol) rotating at 3000 rpm. The spinning was then slowed to 2000 rpm and kept for 50
22
23 s. A glass tube was affixed on top of the coverslip with the help of epoxy glue (Hardman®,
24
25 McMaster-Carr). The epoxy was cured in an oven (110°C) for ca. 1 hour, which also dried the
26
27 sample. The solvent utilized was MeCN and the supporting electrolyte was Bu₄NClO₄ (0.1 M).
28
29 The electrochemical cell was completed by sealing with an inverted septum, which was pierced
30
31 by a non-aqueous Ag/Ag⁺ reference electrode and Pt wire counter electrode. The ITO surface
32
33 served as the working electrode and four ITO sectors on the coverslip could be addressed
34
35 independently. The cell was degassed for at least 1 hour with Ar before measurements. An
36
37 argon-filled balloon was affixed to the sample at all times to ensure an Ar positive pressure within
38
39 the electrochemical cell. Individual MPS-PPV NPs were imaged using a wide-field objective-
40
41 based total internal reflection fluorescence (TIRF) microscopy setup consisting of an inverted
42
43 microscope (IX71, Olympus) equipped with a laser-based TIRF illumination module (IX2-
44
45 RFAEVA-2, Olympus). Samples were excited with the evanescent wave of a 488 nm Ar⁺ laser
46
47 output (Melles Griot), obtained by focusing the collimated laser beam at back focal plane of a
48
49 high numerical aperture (N.A. = 1.45) oil-immersion objective (Olympus PLAN APO 60X) and
50
51
52
53
54
55
56
57
58
59
60

1
2
3 launching the excitation past the critical angle. The laser power measured at the exit of the
4
5 objective was 970 μW . Emission was collected through the same objective and images were
6
7 magnified 2-fold *via* a lens system and then captured on a back illuminated electron multiplying
8
9 charge coupled device (EM-CCD) camera (Cascade II:512B, Roper Scientific). Images were
10
11 spectrally separated by a 640dcxr dichroic mirror to give two distinct emission channels, a green
12
13 channel with $\lambda_{\text{em}} < 640$ nm, and a red channel with $\lambda_{\text{em}} > 640$ nm. A total area of about 66×33
14
15 μm^2 was imaged at any given time. The images were analyzed with custom Matlab and IDL
16
17 scripts that identified diffraction-limited fluorescence spots, registered them in both spectral
18
19 channels and calculated the background-corrected integrated fluorescence intensity for each
20
21 individual NP in either the green or red channel. Electrochemical potential was controlled by a
22
23 CHI600D electrochemical analyzer. The applied bias (E_{app}) and acquired movies were
24
25 temporally synchronized. A cyclic voltammetry potential waveform was applied to the sample,
26
27 the E_{app} were initiated at + 0.53 V and were first swept to the minimum peak potential (either +
28
29 0.03 V (Figure 2) or – 0.97 V (Figure 5)) and then to the maximum peak potential of + 1.03 V.
30
31 Potentials were scanned at a rate of either 50 or 100 mV/s while frames were acquired at a rate of
32
33 10 Hz.
34
35
36
37
38
39
40
41
42

43 RESULTS AND DISCUSSION

44 **Effect of water content in H₂O/THF and H₂O/MeCN mixtures.**

45
46 We prepared CPE NPs by rapidly injecting a CPE aqueous solution into the water-miscible
47
48 organic solvent, either THF or MeCN. During injection individual MPS-PPV chains aggregate or
49
50 collapse to form CPE NPs. This nano-precipitation process is analogous (albeit with opposite
51
52 polymer and solvent polarities) to the method reported to produce neutral conjugated polymer
53
54
55
56
57
58
59
60

1
2
3 NPs following injection of their THF solutions into H₂O.²⁷ This reprecipitation method has been
4 extensively used to form conjugated polymer NPs, but is far less common for the case of
5 conjugated polyelectrolytes.²⁸⁻³⁰ Nanoparticle formation was monitored via dynamic light
6 scattering (DLS) analysis of dispersions of MPS-PPV in various H₂O/THF and H₂O/MeCN
7 mixtures, ranging from 0.5% to 100% v/v in water (see Table 1 and Table S1). Nanoparticles of
8 MPS-PPV 212 nm in diameter (by DLS) were recorded at 0.5% H₂O/THF v/v. These NPs were
9 also observed in scanning electron microscopy (SEM) micrographs, although we recorded a
10 smaller average size of 124 nm in diameter (Figures 1 and S1). The difference in size
11 presumably arises due to swelling of the NPs in solution for the DLS experiments. Increasing the
12 water content above 0.5% v/v led to a reduction of the recorded size of the NPs in our DLS
13 studies as better solubilization of the CPEs takes place. At water contents above 15% v/v, the
14 scattering counts were below the detection limit of our setup.

15
16
17
18
19
20
21
22
23
24
25
26
27
28
29
30
31
32 The chain conformation of CPEs was extremely sensitive to nanoparticle preparation
33 conditions. We observed a broad, red-shifted fluorescence at very low water content in
34 water/THF solutions, in the range of 0.5-2.5% H₂O v/v, see Table 1 and Figure 1. At higher
35 water contents (5-50% H₂O v/v) the fluorescence intensity was significantly enhanced (up to 10-
36 fold increase) and the emission spectrum, while still broad, was markedly blue-shifted (up to 80
37 nm). Similar trends were observed for MPS-PPV dispersed in H₂O/MeCN solutions, however the
38 fluorescence enhancements were not nearly as pronounced as those in THF presumably because
39 MeCN is a poor solvent for the PPV backbone (see Figure S2). Changes in absorption spectra
40 with increasing H₂O content were also consistent with conformational changes. A decreasing
41 proportion of red-absorbing sites were recorded in going from 0.5 to 50% H₂O by volume in
42 THF (see Figure S3). At the lowest water content, broadening of the absorption peak, indicative
43
44
45
46
47
48
49
50
51
52
53
54
55
56
57
58
59
60

of a large distribution of conjugation lengths and/or chain conformations, was observed. Also recorded was a red-absorbing tail which extended up to ~ 600 nm.

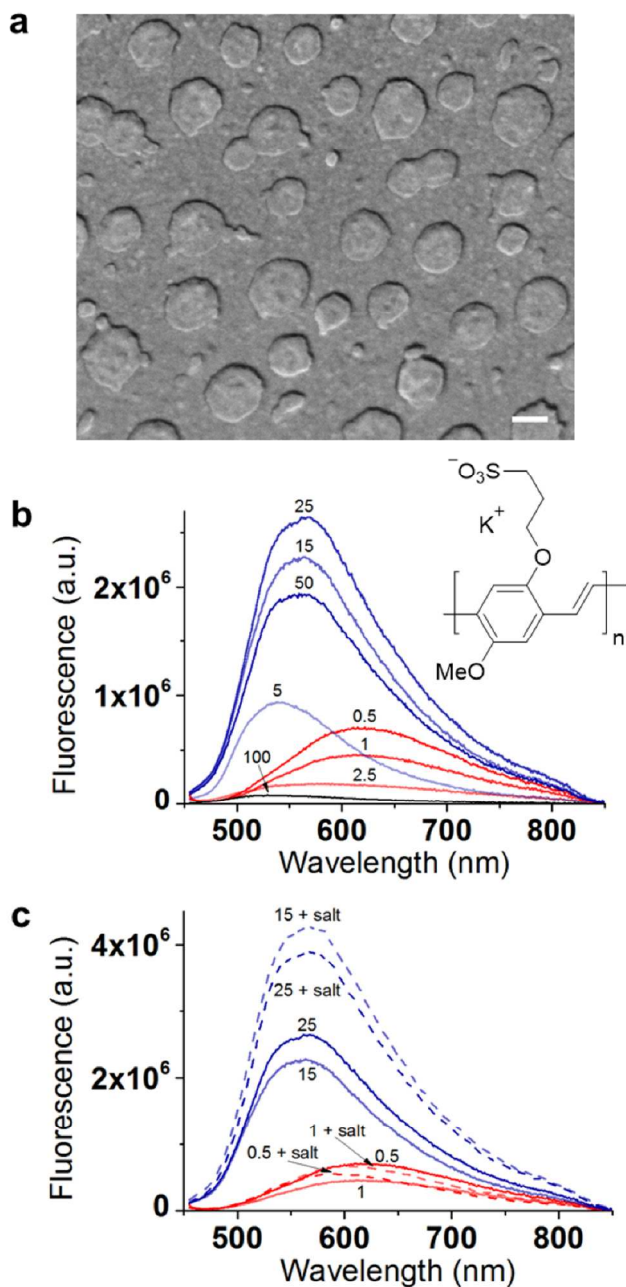


Figure 1. a) SEM image of MPS-PPV NPs (formed in 0.5% H₂O v/v in THF solution) dispersed on a glass coverslip. See sample preparation details in the text. Scale bar is 100 nm. Fluorescence emission properties of MPS-PPV dispersed in various H₂O/THF solutions (b) before (solid lines)

and (c) after (dashed lines) addition of 100 mM Bu_4NClO_4 as a powder, $\lambda_{\text{ex}} = 450$ nm in both cases. Panel (c) also shows spectra of two samples before addition of Bu_4NClO_4 (solid lines) to allow for direct comparison. The water content (in % v/v) is indicated near the fluorescence maximum in each trace. The low water regime ($\leq 2.5\%$ H_2O by volume) is shown in red while the high water regime ($\geq 5\%$ H_2O by volume) is shown in blue. Fluorescence in water-only solution is shown in black. Shown in the inset is the chemical structure of MPS-PPV.

Table 1. Spectroscopic and DLS characterization of MPS-PPV dispersions in $\text{H}_2\text{O}/\text{THF}$ solutions.

		MPS-PPV + H_2O + THF			MPS-PPV + H_2O + THF + Bu_4NClO_4		
$\text{H}_2\text{O}^{\text{a}}$ (%v/v)	$n_{\text{H}_2\text{O}}/n_{\text{THF}}$	$\lambda_{\text{em}}^{\text{b}}$ (nm)	Diam. (nm) ^c	Relative emission ^b	$\lambda_{\text{em}}^{\text{b}}$ (nm)	Diam. (nm) ^c	Relative emission ^b
0.5	0.02	622	212	9	588	1900	7
1.0	0.05	613	146	6	605	3300	8
2.5	0.12	583	110	3	544	1360	18
5.0	0.24	543	82	9	566	1494	36
15	0.79	557	N/D	24	570	N/D	46
25	1.50	568	N/D	28	571	N/D	42
50	4.50	559	N/D	21	N/A	N/A	N/A
100	-	518	N/D	1	554	N/D	4 ^d

^aIn THF. ^bWavelength corresponding to the maximum of the emission spectrum. The excitation wavelength utilized was 450 nm, and absorption at this wavelength did not vary more than $\sim 10\%$. Emissions intensities are relative to the emission of MPS-PPV in pure water. Absorption and emission intensities of solutions containing particles larger than ~ 300 nm are likely to be affected by the penetration depth of light into the CPE.³¹ ^cAs measured by DLS.

^dSaturated solution of Bu_4NClO_4 in H_2O (concentration $\ll 100$ mM). N/D = not detectable.

1
2
3
4
5
6 Although it is difficult to assign the red fluorescence to a specific emitting species,³² the fact
7
8 that red-absorbing sites are formed in our system (see Figure S3) indicates an increase in the
9
10 average conjugation length and/or the formation of aggregates. While more specific assignment
11
12 of the red-emitting species is beyond the scope of the present study, it is important to recall that
13
14 the origin of red-shifted fluorescence in conjugated polymers has been previously attributed
15
16 either to an increase in the conjugation length and/or to the formation of interchain species.³³⁻³⁸
17
18 Here 'interchain species' denotes a group of non-neighboring chromophore segments in the
19
20 polymer backbone that are in contact.^{18, 39} Following the nomenclature defined by Schwartz,¹⁸
21
22 the term aggregates refer to interchain species that interact in the ground state. Excimers in turn
23
24 refers to interchain species that interact exclusively in the excited state, resulting in changes in
25
26 the fluorescence, but not the absorption spectra.⁴⁰
27
28
29
30

31
32 Insight on the CPE chain conformation can be gained by comparing the observed spectral and
33
34 NP size trends (Table 1). Increasing the water content from 0.5% to 15% v/v leads to smaller
35
36 NPs with blue-shifted fluorescence. With increasing water content the CPE becomes relatively
37
38 well solvated and interchain interactions between MPS-PPV chains are less prominent, leading
39
40 to a blue-shift in the absorption and fluorescence spectra and a marked increase in emission
41
42 intensity. Similar observations have been made with MPS-PPV dispersed in mixtures of H₂O and
43
44 DMSO (a good solvent for MPS-PPV chains), where a large fluorescence enhancement in pure
45
46 DMSO were recorded and assigned to the absence of exciton-exciton annihilation within the
47
48 PPV backbone.⁴¹ We postulate that, at very low water content, MPS-PPV chain segments are
49
50 straightened out and bury the charged side groups within water rich pools, effectively increasing
51
52 the average conjugation length of the chromophores.¹⁸ In turn, the extended conformation allows
53
54
55
56
57
58
59
60

1
2
3 for better π - π stacking between chromophores promoting the formation of interchain species
4 (aggregates and excimers) and NPs. Increased interchain interactions lead to red-shifted (and
5 weak) fluorescence as low-energy emissive sites (and non-emissive sites) are eventually
6 populated upon extensive energy transfer.⁴²⁻⁴⁴
7
8

9
10 We next explored the role that the large hydrophobic counterion tetrabutylammonium
11 perchlorate (Bu_4NClO_4) has on the spectroscopic properties of MPS-PPV (Figure 1c). The
12 information is relevant to our single molecule/particle spectroelectrochemistry studies where
13 Bu_4NClO_4 was used as the supporting electrolyte (*vide infra*). In the presence of Bu_4NClO_4 , we
14 observed a significant increase in fluorescence when MPS-PPV was dispersed in 15% H_2O v/v in
15 THF. A maximal 46-fold fluorescence enhancement was observed compared to MPS-PPV
16 dispersed in neat H_2O with no Bu_4NClO_4 . These observed changes in luminescence, also
17 recorded in $\text{H}_2\text{O}/\text{MeCN}$ solutions, point to better solvation of MPS-PPV polymer chains when an
18 organic cation is added to a $\text{H}_2\text{O}/\text{organic}$ solvent mixture rich in the organic fraction. The alkyl
19 groups in the large counterion act as spacers that effectively separate polymer chains and inhibit
20 their contact.⁴⁵ The greasy counterions may additionally minimize the tendency of CPEs towards
21 packing with each other to reduce contact with water, exerting a surfactant effect. At water
22 contents of 1% or lower, the emission enhancement of MPS-PPV was significantly smaller,
23 indicating that Bu_4NClO_4 did not significantly alter the NPs structure under these conditions. A
24 similar effect is expected under the anhydrous conditions we employed in our single molecule
25 measurements described below.
26
27
28
29
30
31
32
33
34
35
36
37
38
39
40
41
42
43
44
45
46
47
48
49

50 **Single Molecule Spectroelectrochemistry of MPS-PPV particles.**

51
52 In order to unravel the role that chain conformation plays in the differential optoelectronic
53 behavior of individual MPS-PPV NPs we developed a two-color single-molecule
54
55
56
57
58
59
60

1
2
3 spectroelectrochemistry (SMS-EC) technique to correlate changes in either green
4 (coiled/deaggregated) or red (extended/aggregated) emission with applied electrochemical bias
5 (E_{app}).⁴⁶ Specifically, NPs were spin cast onto an ITO coated glass coverslip (working electrode)
6 and an air tight electrochemical cell was assembled with reference and counter electrodes (Figure
7 2a). Samples were next mounted on a total internal reflection fluorescence microscope (TIRFM).
8 Images were recorded at 10Hz rate in an electron multiplied CCD camera (EMCCD) while
9 sweeping the external potential E_{app} in the electrochemical cell. Tens of surface immobilized NPs
10 could thus be followed over time. Intensity vs. time trajectories for each individual particle in
11 both color channels were constructed from the stack of images (Figure 2b). We studied NPs
12 formed in 0.5% v/v H₂O in THF as the solution properties of these NPs, characterized by a high
13 level of interchain interactions, are expected to be representative of those corresponding to NPs
14 deposited on a surface and monitored in dry MeCN solutions.

15
16
17
18
19
20
21
22
23
24
25
26
27
28
29
30
31
32 In the following we first describe our results for a ‘narrow’ E_{app} range (+ 0.03 to + 1.03 V vs.
33 NHE, Figure 2) and discuss the phenomena occurring in this E_{app} range (thermal electrochemical
34 oxidation and photoinduced electron transfer). Results obtained for a wider E_{app} range, keeping
35 the maximum at + 1.03 V but extending on the reductive side to – 0.97 V (Figure 5), are next
36 presented and the new processes occurring (asymmetric fluorescence enhancement and
37 differences in hole filling) are discussed in the context of polymer morphology.

38
39
40
41
42
43
44
45
46 **Results for + 1.03 V $\geq E_{app} \geq$ +0.03 V.** Shown in Figure 2 are representative normalized
47 fluorescence intensity trajectories for a single particle and subensembles (average of selected
48 single particle trajectories), recorded in both the green and red channel upon scanning the E_{app}
49 linearly over time between + 0.03 V and + 1.03 V vs. NHE (see Figure S4, for non-normalized
50 intensities). Starting with an open circuit, applying a potential of + 0.53 V (at time = 4 s) resulted
51
52
53
54
55
56
57
58
59
60

1
2
3 in a slight reduction of fluorescence intensity (I_f) in the green channel, yet a marked one in the
4 red channel. As E_{app} was swept towards 0 V (up to time = 11 s), all particles showed a reversible
5
6
7
8 I_f enhancement in the red channel. For the green channel a subset of particles (ca. 50%) showed
9
10
11 I_f enhancements, albeit smaller in relative magnitude to those observed in the red channel (Figure
12
13 2d). The changes in I_f are reversed as the bias is swept linearly over time from + 0.03 V back to
14
15 + 0.53 V (from 11 s to 16 s). In contrast, the remaining particles showed negligible changes in I_f
16
17 (Figure 2e).

18
19
20 At the onset E_{app} of $\sim + 0.54$ V and increasing until + 1.03 V a sharp quenching of the
21
22 fluorescence intensity was observed followed by a steady recovery upon scanning E_{app} back from
23
24 + 1.03 V to + 0.54 V (gray regions in Figure 2, corresponding to potentials $\geq + 0.54$ V). The
25
26 quenching and recovery in this bias range were equally prominent in both the green and red
27
28 channels. However, for both channels, the intensity did not fully recover at the end of the first
29
30 cycle. This is probably the result of either permanent photodamage to the polymer or irreversible
31
32 reactions taking place after extensive electrochemical oxidation of MPS-PPV.⁴⁷ Similar
33
34 conclusions applied to I_f trajectories recoded during a second potential applied immediately
35
36 following the first cycle (see Figures S5 and S6).
37
38
39
40
41
42
43
44
45
46
47
48
49
50
51
52
53
54
55
56
57
58
59
60

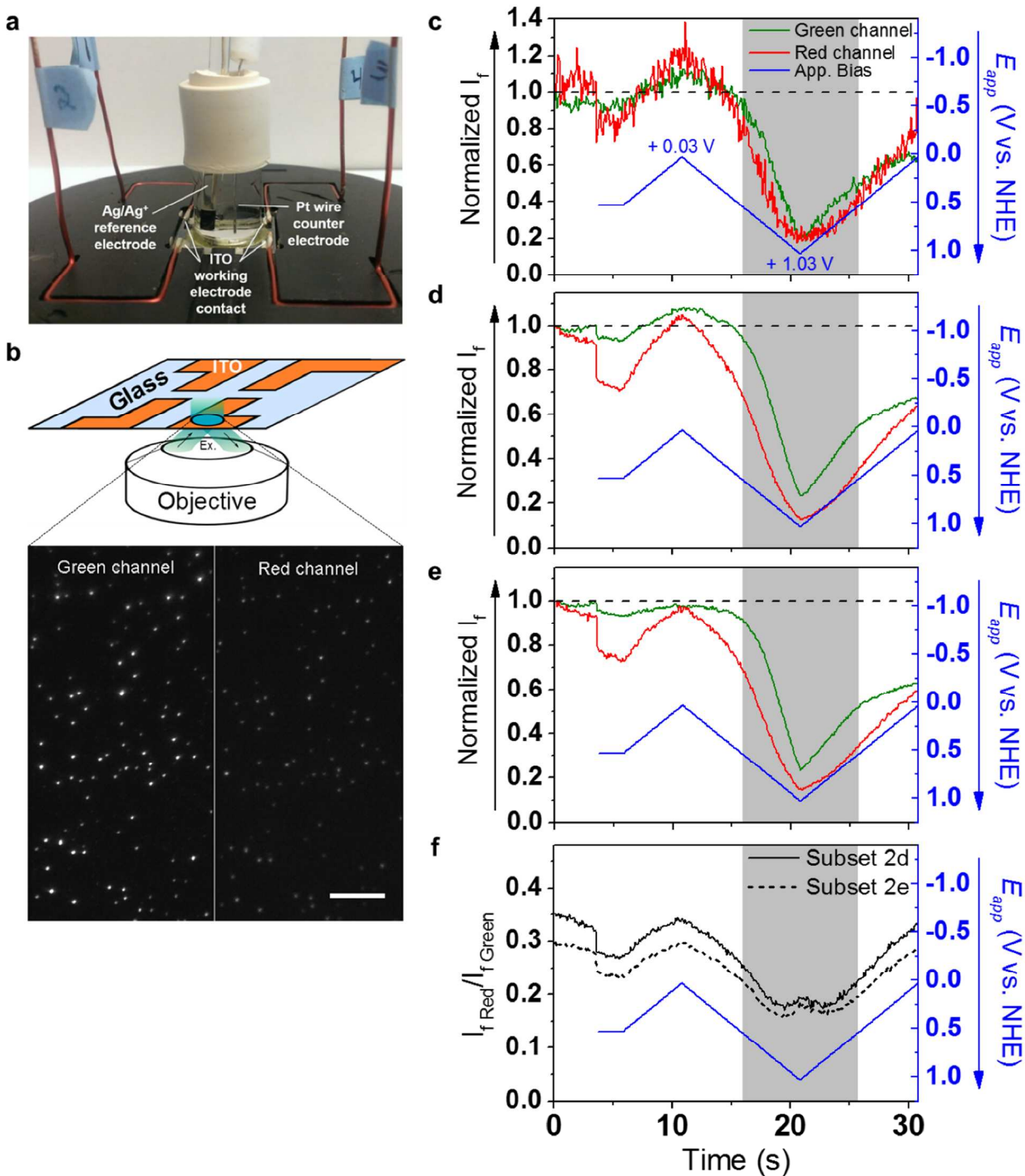


Figure 2. Effect of applied bias on MPS-PPV NP fluorescence as measured by TIRFM based color-sensitive SMS-EC. a) Photograph of the SMS-EC cell. b) Cartoon illustrating the coverslip with four independent ITO working electrodes and the evanescent optical excitation. The

1
2
3 resulting emission from individual nanoparticles is collected by the objective and relayed to the
4 chip of an EM CCD camera for image capture. One acquired frame is shown below depicting
5 real data in the green and red channels. The scale bar is 10 μm . c) Chromatically-resolved (green
6 and red) SMS-EC single particle fluorescence intensity trajectories normalized to the initial
7 fluorescence intensities. Panels d) (47% of the total) and e) (53% of the total) show normalized
8 ensemble fluorescence intensity trajectories for two subsets of NPs showing differing
9 enhancement behavior in the green channel under E_{app} in the region between + 0.03 V and + 0.54
10 V. Dashed lines corresponding to the initial intensities are visual guides to emphasize the
11 changes in intensity. f) Non-normalized red-to-green fluorescence intensity ratios for NP subsets
12 presented in d) and e). Peaks seen at E_{app} near + 1 V are artifacts resulting from the fluorescence
13 intensity in the red channel dropping near background levels. A total of 68 NPs were analyzed.
14 Time intervals where E_{app} was > + 0.54 V are highlighted in grey.

15
16
17
18
19
20
21
22
23
24
25
26
27
28
29
30
31
32
33
34
35 The marked I_f quenching observed as E_{app} is swept above the + 0.54 V onset potential and the
36 recovery recorded in the return sweep are consistent with the reversible electrochemical
37 oxidation of the ground state of MPS-PPV. Exciton quenching has been observed in similar
38 studies conducted on MEH-PPV, the non-ionic counterpart of MPS-PPV, upon hole injection
39 and formation of a radical cation.⁴⁸ The onset p-doping potentials of other 2,5-dialkoxy-
40 substituted PPVs have been reported to be in the range of + 0.85 to + 0.91 V vs. NHE,⁴⁹⁻⁵⁰
41 consistent with our assignment of oxidation of MPS-PPV NPs at potentials more positive than +
42 0.54 V (see discussion below for $E_{1/2}$ values) and indicative of the high sensitivity of
43 photoluminescence intensity to the presence of holes (radical cation species) in this CPE.
44 Alternatively, electric field-induced fluorescence quenching has been observed for conjugated

1
2
3 polymer chains.⁵¹⁻⁵³ We do not expect our data to be significantly affected by electric-field
4 effects since the electric field generated at the electrode/solution interface is suppressed at
5 distances beyond 1 nm (the extent of the electrochemical double layer) by the high concentration
6 of supporting electrolyte. The charges present in MPS-PPV would also result in screening of the
7 electric field within the NPs. It is possible that the emitting sites located at the interface of the
8 electrode exhibit electric field-induced quenching, although these are presumed to be a small
9 fraction of the total emitting sites of the NPs. Most importantly, the polarity of the applied bias
10 influences the fluorescence changes and is inconsistent with a purely electric field-driven
11 process.
12
13
14
15
16
17
18
19
20
21
22
23

24
25 Importantly, the distribution of potentials at which I_f is quenched by half relative to the initial
26 $I_f(E_{1/2})$ and the I_f modulation depth we recorded were very similar for all particles in both color
27 channels. The $E_{1/2}$ for each particle and for both color channels was very narrow, ca. ± 0.03 V.
28 The mean $E_{1/2}$ recorded in the red channel, $\sim +0.8$ V, was slightly smaller than that recorded for
29 the green one, $\sim +0.9$ V, see Figure 3. The smaller value of $E_{1/2}$ recorded in the red vs. green
30 channel, while initially surprising, is readily rationalized considering that segments with an
31 average longer conjugation (red-emitting sites) are easier to oxidize than those with shorter
32 conjugation segments (green-emitting sites).⁵⁴ As the values of $E_{1/2}$ relate to the ground state
33 oxidation process,⁴⁸ we conclude that a significant portion of the red-emitting sites are present in
34 the ground state (i.e. they are not excimers). This is in line with observation of red-absorbing
35 sites in the MPS-PPV NPs (Figure S3).
36
37
38
39
40
41
42
43
44
45
46
47
48
49

50
51 The I_f modulation depth we recorded was ca. 80% (75% in the green channel, 85% in the red
52 channel) relative to the initial I_f . The narrow distribution of $E_{1/2}$ along with the observation that
53 all particles showed high I_f modulation depth indicate that all the studied particles were in good
54
55
56
57
58
59
60

1
2
3 ohmic contact with the ITO working electrode.^{26, 48} The observation that the quenching
4 modulation depth was ~ 80% within a relatively narrow 0.5 V bias range above the quenching
5 onset indicates that holes injected in these NPs were significantly electrostatically screened from
6 each other, presumably by the sulfonate side groups along the polymer backbone. This screening
7 permitted the efficient injection of multiple holes necessary to account for the large modulation
8 depth in a ca. 100 nm diameter nanoparticle, within the short bias range experimentally recorded.
9
10 The large fluorescence intensity modulation in the short bias range compares to the results
11 recorded with small (25nm diameter) NPs of MEH-PPV, where 98% fluorescence quenching
12 was achieved within a 0.3 V range.⁴⁸ Solvent penetration and external ion screening were called
13 upon to justify the narrow range and large modulation with MEH-PPV small particles. These
14 factors would also be operational in the ionic MPS-PPV.
15
16
17
18
19
20
21
22
23
24
25
26
27
28
29
30
31
32
33
34
35
36
37
38
39
40
41
42
43
44
45
46
47
48
49
50
51
52
53
54
55
56
57
58
59
60

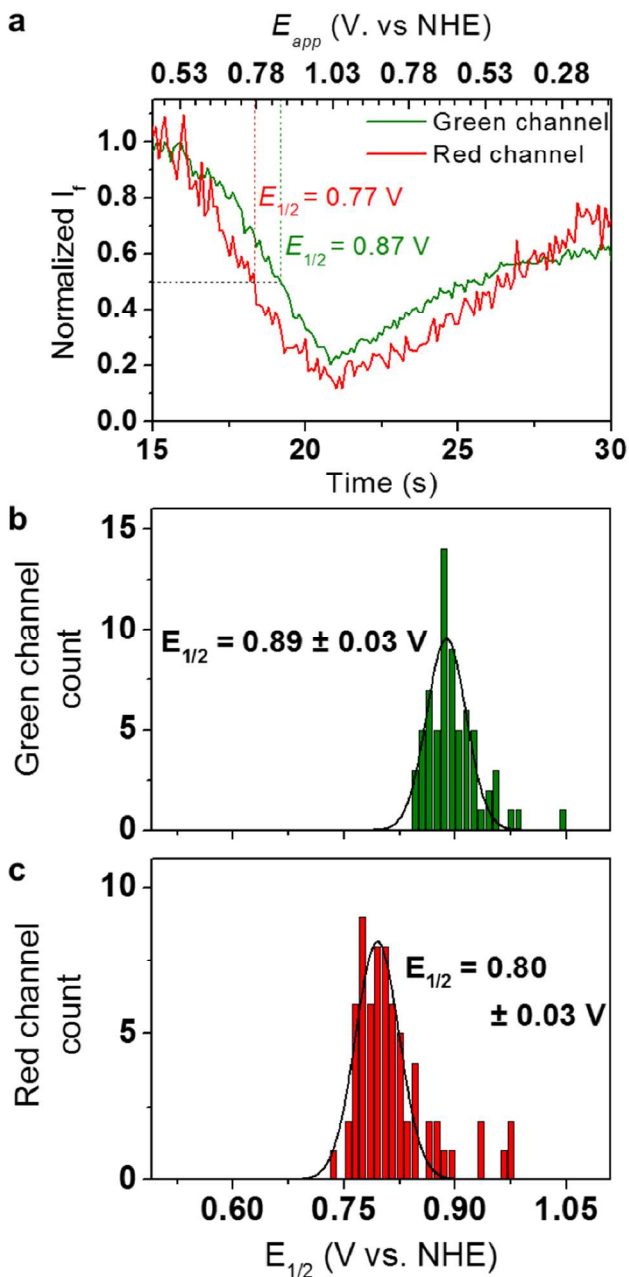


Figure 3. Distributions of $E_{1/2}$ values determined from single particle intensity-time trajectories.

a) Representative chromatically-resolved (green and red) single particle fluorescence intensity trajectories recorded in our two-color SMS-EC setup. The I_f recorded at + 0.54 V, before the first oxidative quenching event, was taken to be 1. The $E_{1/2}$ is the applied bias where the intensity dropped by half. The center and width of the Gaussian distributions were taken to represent the

1
2
3 mean and the standard deviation of $E_{1/2}$ values. Panels b) and c) display data extracted from the
4
5 green and red channels for both NP subsets shown in Figures 2d and 2e.
6
7

8
9 Having unraveled the origin of the fluorescence intensity quenching at $E_{app} \geq +0.54V$ as
10 thermal hole injection we next discuss the observed modulation in I_f for E_{app} between + 0.54 V
11 and + 0.03 V (white regions of Figures 2c-f). Specifically, we address first the origin of the I_f
12 enhancement with reduction in E_{app} , and next the particle-to-particle heterogeneous behavior
13 observed for the green channel and the differential relative amplitude of I_f for the two channels
14 (green vs red).
15
16
17
18
19
20
21

22
23 Excited state electrochemical oxidation and reduction processes (photoinduced electron
24 transfer (PeT) from (to) photoexcited MPS-PPV to (from) ITO) are both plausible in the
25 potential range between + 0.54 V and + 0.03 V, resulting in the quenching of polymer emission.
26
27 In turn, no ground state redox process is known to occur for MPS-PPV in this bias range. We
28 thus assigned the observed voltage-induced intensity modulation in the above potential range to
29 changes in the rate of photoinduced redox processes from photoexcited MPS-PPV (see Figure 4).
30
31 Lowering E_{app} (raising the Fermi level (E_F) of ITO) should decrease the rate constant for
32 photoinduced oxidation (k_{ox}^*) concomitant with a reduction in the driving force for the oxidation
33 of MPS-PPV,. In turn, the rate constant for photoinduced reduction (k_{red}^*) should increase as E_{app}
34 is lowered. Considering the initial segment of the intensity-time trajectories, engaging the bias at
35 + 0.53 V (Figures 2c-e, time = 4 s) leads to a drop in the I_f of the nanoparticles compared to the
36 open circuit case. This is consistent with an overall increase in the PeT rate (sum of k_{ox}^* and k_{red}^* ,
37 Figure 4). Subsequent lowering of the bias enhanced the I_f , in line with a relatively smaller
38 increase of k_{red}^* compared to the decrease of k_{ox}^* under these conditions. The observation that a
39 nanoparticle I_f recorded under applied bias may surpass the I_f recorded at open circuit further
40
41
42
43
44
45
46
47
48
49
50
51
52
53
54
55
56
57
58
59
60

signals that PeT was already operational at open circuit, resulting in static quenching of the polymer emission.⁴⁸

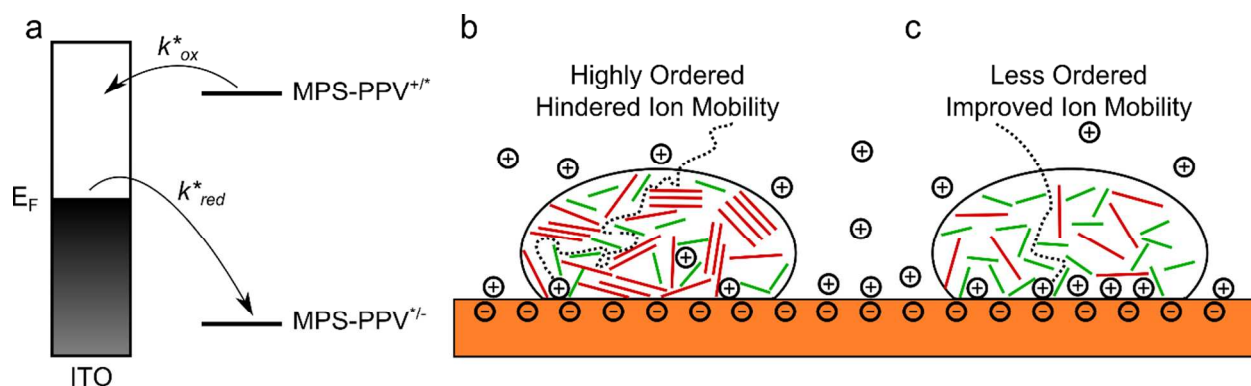


Figure 4. Cartoons illustrating: (a) state energy diagram for the MPS-PPV/ITO system. In SMS-EC experiments the energy of the ITO Fermi level (E_F) is modulated by an external bias. (b,c) cartoon rendering the hypothetical ordering of MPS-PPV NPs on an ITO electrode, where the polymer backbone is either (b) extended and aggregated or (c) coiled and deaggregated.

It is interesting to note that different results were obtained for the modulation of I_f with E_{app} for charged vs. uncharged conjugated polyphenylene vinylene (PPV) polymers in the bias range between 0 V and + 0.54 V. These discrepancies underscore the role of side groups in tuning the photophysical properties of the PPV parent backbone. Specifically, previous SMS-EC studies conducted on MEH-PPV NPs showed a linear modulation of I_f with E_{app} under mild electrochemical potentials.⁴⁸ The results however showed a drop in intensity with decreasing E_{app} , contrary to our results with MPS-PPV. With MEH-PPV it was concluded that excited state reduction of the polymer chains was the dominant pathway, i.e., with decreasing bias (raising the E_F of ITO) the increase in k_{red}^* and ensuing quenching is more important than the drop in k_{ox}^*

1
2
3 that would lead to enhanced I_f . Our studies with MPS-PPV are in line with excited state
4 oxidation being the dominant process at play in this bias range. The change of regime from
5 overall photoinduced reduction (MEH-PPV) to overall photoinduced oxidation (MPS-PPV) is
6 possibly related to the lowering of the barrier to electron injection into ITO due to the dipole
7 created at the ITO surface from negatively charged side groups on MPS-PPV.⁵⁵⁻⁵⁷
8
9
10
11
12
13
14
15
16
17

18 Following our discussion on thermal and photoinduced redox processes accounting for the
19 modulation of I_f in the bias range between 0 V and + 1 V, we next address the particle-to-particle
20 heterogeneous behavior observed for the green channel and the differential relative amplitude of
21 I_f for the two channels (green vs red) (see Figure 2). These experimental observations may be
22 rationalized by considering the effects of ion motion through the MPS-PPV NPs and the extent
23 of aggregation and energy transfer characterizing green and red emissive sites as it is described
24 in detail below. Briefly, the rearrangement of ions that occurs when a potential is applied results
25 in the formation of a double layer and to changes of the electric field in the vicinity of the
26 electrode.⁵⁸ The resulting reorganization affects the kinetics of photoinduced redox processes
27 between ITO and MPS-PPV.
28
29
30
31
32
33
34
35
36
37
38
39

40 We postulate that the ease of external ion migration through the NPs will dictate the sensitivity
41 of I_f to E_{app} in a potential window where the only mechanism that modulates I_f is PeT. Higher
42 external ion mobility and easier chain reorganization should lead to better screening of the
43 electric field generated at the working electrode and a lower sensitivity of I_f to changes in
44 potential. We note that the indistinguishable ground state oxidative quenching behavior recorded
45 for the subset of NPs in Figures 2d and 2e (see also Figure S9b) is consistent with similar
46 polymer chain interactions in both systems, including charge transport characteristics. In this
47
48
49
50
51
52
53
54
55
56
57
58
59
60

1
2
3 regard, the differential behavior between subsets in the green color channel should thus be
4
5 dominated by external factors such as ion percolation/mobility. We therefore postulate that NPs
6
7 with a marked green channel I_f modulation in the + 0.03 V to + 0.54 V range (subset 2d; also see
8
9 Figure S7) are characterized by a lower external ion mobility (larger sensitivity to E_{app}) than
10
11 those that show low modulation within this potential range (subset 2e).
12
13
14

15 The differential relative amplitude of I_f for the two channels (green vs. red) may be
16
17 rationalized considering the extent of aggregation and energy transfer characterizing green and
18
19 red emissive sites. Compared to green-emitting sites, red-emitting sites are thought to be better
20
21 packed and have stronger interchain interactions,⁵⁹⁻⁶⁰ resulting in better charge transport²² and
22
23 faster energy transfer.^{19, 61} Note that in this context *charge transport* refers to the movement of
24
25 charge (radical anions or cations) within the conjugated polymer material by means of a hopping
26
27 mechanism which takes place among nearby chain segments (charge carriers) belonging to the
28
29 same chain or different chains.⁶² Under applied electrochemical potentials we postulate that
30
31 external ion migration through open spaces in a structure dominated by red-emitting sites is
32
33 difficult because the corresponding chains are closely packed and have less freedom of motion
34
35 (Figure 4c).⁶³ The electric field generated at the working electrode is thus poorly screened for
36
37 red-emissive sites resulting in a high sensitivity of the associated I_f to changes in E_{app} for a
38
39 potential window where the only active mechanism is PeT (i.e. marked I_f modulation with E_{app} in
40
41 the + 0.03 V to + 0.54 V range, Figures 2 and 5). We further note that the better light harvesting
42
43 ability of red-emitting over green-emitting sites, due to their intrinsically higher energy transfer
44
45 efficiency, would lead to a strong amplification of the I_f quenching via excited state redox
46
47 processes. In other words, the intrinsic longer exciton diffusion length of red-emitting sites
48
49 results in a higher fraction of excitons reaching the electrode for PeT relative to green-emitting
50
51
52
53
54
55
56
57
58
59
60

1
2
3 sites. The combined action of poorer external ion mobility (lesser screening) and better energy
4 transfer results in a stronger relative I_f modulation for red emissive vs. green emissive sites
5 (Figures 2f, 5d), and is in line with the higher modulation depth recorded for red-emitting sites as
6 previously described (Figure 3). In line with better energy transport, red-emitting sites are more
7 prone to irreversible photodamage following prolonged imaging, as can be observed from the
8 larger relative drop in I_f for red-emitting sites vs. green-emitting sites before engaging the
9 applied bias and after disengaging the applied bias (see Figures S5 and S6).

10
11 The SMS-EC experiments further reveal a faster (non hysteretic) response to E_{app} in red- vs.
12 green-emitting sites observed as E_{app} are swept to more negative values (up to - 0.97 V) (vide
13 infra, see also Figure 5e). This phenomenon could also be explained in terms of better contact
14 between red sites and ITO, and/or higher charge mobility within their characteristically highly
15 aggregated backbone.

16
17 Altogether, the above observations reveal that ion mobility, in addition to PPV backbone
18 aggregation, play a crucial role in determining the interfacial (ITO/MPS-PPV) charge transfer
19 dynamics of the system.

20
21 **Results for + 1.03 V $\geq E_{app} \geq - 0.97$ V.** Larger I_f enhancements were recorded, in both red and
22 green channels when E_{app} was scanned to negative peak values of - 0.97 V (Figure 5). Two
23 differing behaviors were observed at these negative biases. One subset of NPs (~50% of the total
24 of 76 NPs monitored) displayed a linear response in I_f with E_{app} in the range of + 0.54 V to - 0.97
25 V (Figure 5a) while a second subset showed asymmetric I_f response for E_{app} lower than - 0.68 V
26 (regions in purple in Figure 5), particularly evident in the green channel (Figure 5b). We draw
27 comparisons between NP subsets 2d and 5a (2e and 5b) that show a higher (lower) sensitivity of
28 I_f to E_{app} . When slowing the potential scan rate by half, to 50 mV/s, all particles showed a single
29

behavior (Figure 5c): specifically, a small change of I_f for potentials between -0.68 V and $+0.54$ V and a sharp I_f enhancement for $E_{app} < -0.68$ V. This is the same behavior observed for the subset of particles presented in Figure 5b.

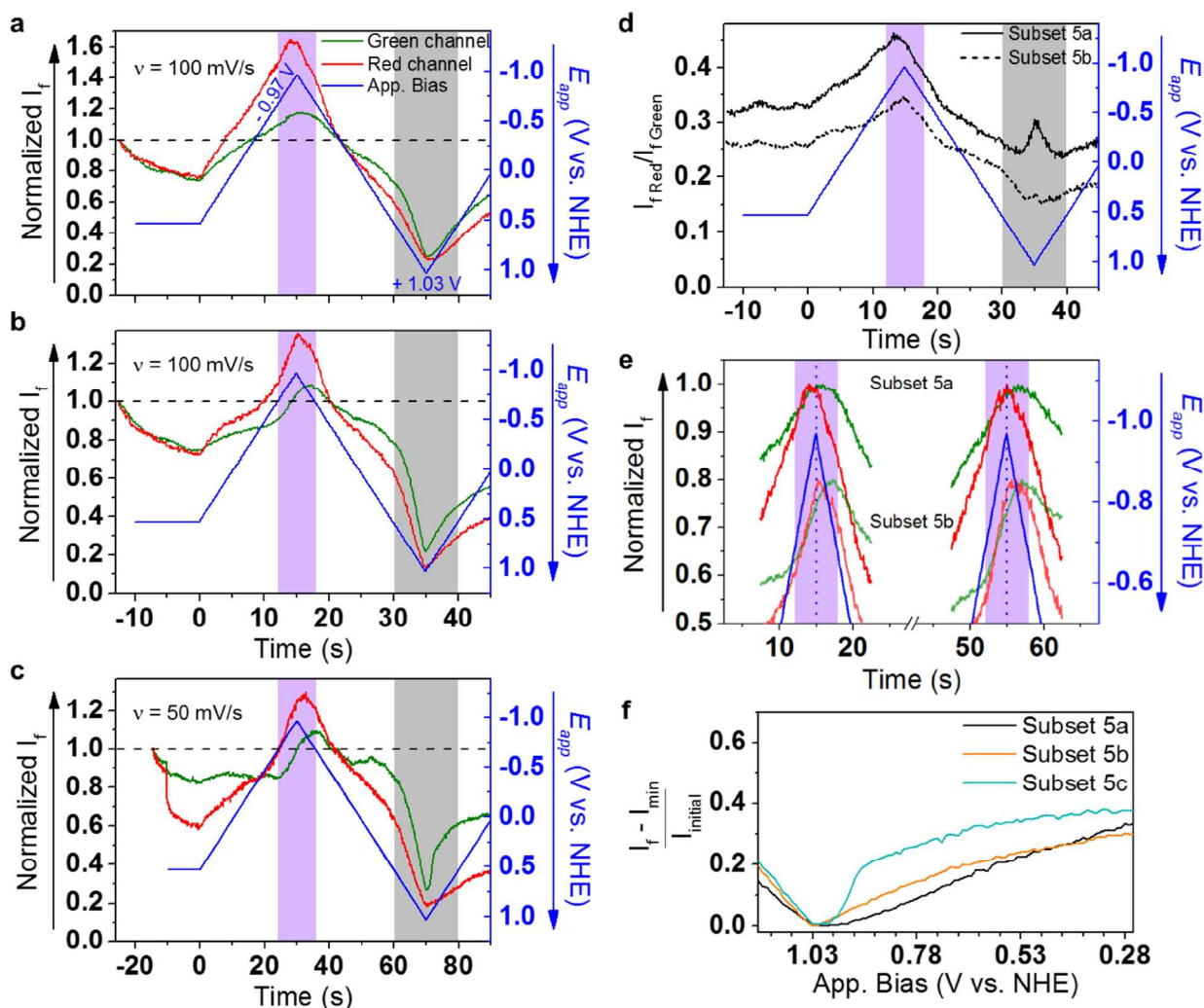


Figure 5. MPS-PPV NP fluorescence as measured by two-color SMS-EC showing the effect of negative applied biases ($-0.97 \leq E_{app} \leq +1.03$ V). (a and b) Average time trajectories normalized to the initial intensities of two subsets of NPs imaged in the same experiment and showing differing behavior at a potential scan rate of 100 mV/s. a) NPs where I_f is highly sensitive to changes in E_{app} . b) NPs that show an asymmetric I_f enhancement at an onset of ~ -0.68 V. c)

1
2
3 Results for MPS-PPV NPs when the potential scan rate is reduced to 50 mV/s, normalized to the
4 initial intensities. Only one type of NP behavior is seen ($n = 37$ particles). d) Non-normalized
5 red-to-green fluorescence intensity ratios for NP subsets presented in a) and b). Peaks seen at
6 E_{app} near + 1 V are artifacts resulting from the fluorescence intensity in the red channel dropping
7 near background levels. e) Changes in normalized fluorescence intensity relative to the
8 maximum I_f for the NP subsets shown in a) and b). The traces of subset 5b are offset by 0.2 units
9 to increase clarity. e) Changes in normalized fluorescence relative to the minimum I_f recorded in
10 the green channels at the first positive peak potential for NP subsets shown in a), b) and c). Data
11 shown corresponds to time = 25 – 45 s for subsets 5a and 5b, and time = 50 – 70 s for subset 5c.
12 Time intervals where E_{app} is $> + 0.54$ V are highlighted in grey, while those where E_{app} is $< -$
13 0.68 V are highlighted in purple.
14
15
16
17
18
19
20
21
22
23
24
25
26
27
28
29

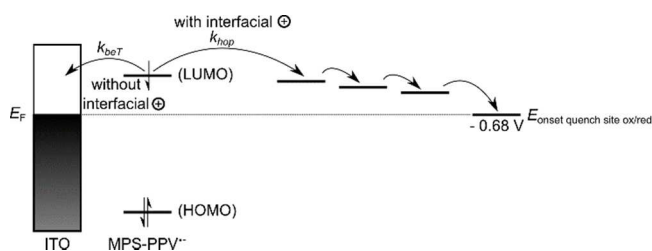
30 The observed asymmetric behavior at negative bias (purple region in Figure 5) is consistent
31 with the thermal reduction of otherwise non-emissive quenched sites. The reduction potential
32 onset of MPS-PPV is expected to be in the range of - 1.3 V to - 1.55 V vs. NHE by comparison
33 to other 2,5-dialkoxy-substituted PPVs.⁴⁹⁻⁵⁰ Considering this redox potential and also that the
34 redox process we observed at $E_{app} < - 0.68$ V led to an increase in I_f , as opposed to intensity
35 quenching expected from the formation of MPS-PPV radical anions, we conclude that a species
36 different to pristine MPS-PPV is undergoing reduction at E_{app} more negative than - 0.68 V.
37
38
39
40
41
42
43
44
45

46 We postulate that non-emitting, photooxidized sites along the MPS-PPV backbone were
47 transiently modified under the reductive potentials ($< - 0.68$ V) to non-quenching sites, giving
48 rise to the sharp I_f increase. It is well known that PPV polymers photooxidize easily resulting in
49 reduced photoluminescence. It is likely that electrochemical reduction of such quenching sites
50 would restore the I_f of the MPS-PPV polymer.⁶⁴ Importantly, fluorescence studies on individual
51
52
53
54
55
56
57
58
59
60

1
2
3 MEH-PPV chains suggested that reversible fluorescence restoration is possible at reductive
4 potentials, but only for photooxidized polymer.⁶⁵⁻⁶⁶ It has been suggested that the photoproducts
5 include species such as dioxetanes or carbonyl defects.⁶⁷⁻⁷¹ Carboxylic acids are also thought to
6 be formed during PPV photooxidation.⁷² Reversibility of the fluorescence enhancement seen
7 previously,⁶⁵ and in this study (in particular Figure 5c, time window 40 – 60 s) are inconsistent
8 with the irreversible nature of the dissociative reduction of aromatic dioxetanes.⁶⁸ Based on the
9 onset potential for the fluorescence enhancement (- 0.68 V), aldehyde reduction is unlikely to be
10 the process at play since the reduction potential of an aldehyde-terminated oligo PV was reported
11 to be - 2.07 V.⁷³ On the other hand, the reduction potential of benzoic acid at ~ - 0.7 V vs.
12 NHE⁷⁴ is in excellent agreement with our observations. It is thus tempting to conclude that
13 carboxylic acid sites are present in the polymer backbone quenching MPS-PPV fluorescence and
14 that they are reversibly reduced at electrode potentials more negative than -0.68 V, restoring the
15 intrinsic polymer fluorescence. A mechanistic overview of the proposed process is detailed in the
16 Supporting Information. Further studies exploring the effect of negative applied biases on the
17 photophysics of (photooxidized) MPS-PPV are warranted to elucidate the nature of quenching
18 sites.

19
20
21
22
23
24
25
26
27
28
29
30
31
32
33
34
35
36
37
38
39
40
41 Differential ion motion through MPS-PPV NPs, previously invoked to explain the distinct
42 response of the green and red channels towards PeT (*vide supra*), may also account for the
43 occurrence of electrochemical reduction of a quenching site in only a single subset of NPs at a
44 scan rate of 100 mV/s. Rapid ion motion in response to lowering of the potential (Figures 5b, 5c)
45 leads to an accumulation of cations at the electrode surface. These cations will stabilize radical
46 anions formed by photoinduced reduction of MPS-PPV and retard the thermodynamically
47 favorable back electron transfer to the ITO (Figure 6). The injected electron will consequently
48
49
50
51
52
53
54
55
56
57
58
59
60

1
2
3 remain longer in MPS-PPV, increasing the probability of the electron to be transported away
4 from the electrode through self-exchange reactions (i.e. hopping mechanism), and reduce a
5 quenching site. On the other hand, if cations cannot accumulate to stabilize the initial radical
6 anion formed near the electrode, only a few sites in the NP will be sampled before fast back
7 electron transfer occurs thus lowering the probability of reductively repairing a quenching site.
8 Our view that the differential characteristics between NPs are due to the relative ease of external
9 ion diffusion is further supported by the observation of a higher proportion of aggregated and
10 ordered red-emitting sites, which impede ion diffusion, in the NP subsets associated with slower
11 ion motion (Subsets 2d, 5a; see Figures 2f, 5d).



34 **Figure 6.** Proposed effect of MPS-PPV/ITO interfacial ions on the electron transport in MPS-
35 PPV NPs. k_{beT} is the rate of back electron transfer from a MPS-PPV radical anion segment
36 (formed upon PeT from ITO to MPS-PPV) to the ITO electrode. k_{hop} is the self-exchange
37 electron transfer rate between MPS-PPV segments, leading to electron mobility in the CPE. The
38 onset energy for reduction of quenching sites is indicated at -0.68 V ($E_{onset\ quench\ site\ ox/red}$) in
39 accordance to experimental observations. Redox potentials for the MPS-PPV $^{\cdot-}$ segment can be
40 roughly approximated to the energy levels of the highest occupied and lowest unoccupied
41 molecular orbitals (HOMO, LUMO) of ground state MPS-PPV.

42
43
44
45
46
47
48
49
50
51
52
53
54 Focusing next our attention on the recovery of I_f recorded as E_{app} is swept from its peak
55 positive value of $+1.03\text{ V}$ towards lower values (e.g. Figure 5a, times 35 s and later), we note

1
2
3
4
5
6
7
8
9
10
11
12
13
14
15
16
17
18
19
20
21
22
23
24
25
26
27
28
29
30
31
32
33
34
35
36
37
38
39
40
41
42
43
44
45
46
47
48
49
50
51
52
53
54
55
56
57
58
59
60

1
2
3 that I_f is both dependent on the scan rate and the subset of NPs analyzed (see Figure 5f). Previous
4
5 studies on MEH-PPV NPs have revealed the presence of deep holes (hole traps) upon
6
7 observation of a slow recovery of I_f following extensive hole injection, similar to our own
8
9 observations.^{26, 48, 75} As E_{app} decreases from the positive potential peak (+ 1.03 V), the MPS-PPV
10
11 fluorescence is restored by filling (electrochemically reducing) holes that were injected in the
12
13 PPV backbone. We observe a faster recovery of I_f , in other words a faster filling of injected
14
15 holes, for the subset of NPs depicted in Figure 5b and previously associated with fast external
16
17 ion migration. Slowing the potential scan rate (subset 5c) results in a larger yield of filled holes
18
19 at a given bias (i.e. a larger relative intensity restoration at a given bias) consistent with better
20
21 responsiveness of external ions to changes in E_{app} . There is a positive correlation between the
22
23 external ion mobility and the charge mobility in the CPE, as has been previously reported.⁴⁵
24
25
26
27
28

29 Surprisingly, neither the differential rate of recovery of I_f nor the I_f peak response time at E_{app}
30
31 = + 0.03 V were observed when the data was collected in the range between + 1.03 V and + 0.03
32
33 V as shown in Figure 2 (see Figure S9). We attribute the discrepancy when compared to the data
34
35 with E_{app} reaching – 0.97 V to the limiting conditions experienced by the polymer environment;
36
37 in the latter case, substantial external ion reorganization is expected in response to the relatively
38
39 large negative bias. The larger changes in E_{app} used for the experiment illustrated in Figure 5 and
40
41 concomitant ion reorganization directly translate to the optoelectronic properties of MPS-PPV.
42
43
44
45

46 In closing, we also considered the effect of particle size on the photophysical properties of the
47
48 CPE NPs. The optical properties of conjugated polymer NPs mostly depend on the conformation
49
50 of the polymer and the nature of the aggregates.²⁸ Size-independent spectroscopic properties
51
52 have been observed for individual MEH-PPV NPs larger than 10 nm in size.⁷⁶ Our SMS-EC
53
54 experiments performed on NPs originating from the same preparation, showed no marked trends
55
56
57
58
59
60

1
2
3 in measured properties e.g., $E_{1/2}$, fluorescence enhancements, and $I_{f\text{ red}}/I_{f\text{ green}}$, (see Figures S10-
4
5
6 12) with respect to NP size. Here the total initial fluorescence intensity of a NP was used as an
7
8 approximate marker of NP size.⁷⁶ Importantly, the changes in spectroscopic properties that
9
10 parallel changes in size when preparing MPS-PPV NPs in differing water contents (Tables 1 and
11
12 S1) are attributed to changes in the polymer chain conformation and interchain interactions. We
13
14 also considered the possibility of surface species playing a role in the heterogeneous
15
16 fluorescence response to E_{app} . Core-shell structures have been observed for oligomeric phenylene
17
18 vinylene aggregates where monomer-like chains emitting blue-shifted fluorescence were found
19
20 on the particle surface.⁷⁷⁻⁷⁸ In principle, it is possible that the green-emitting sites we observed
21
22 are preferentially located near the surface of the NPs yet the small (sub-diffraction) size of our
23
24 particles does not allow us to directly confirm this possibility. Under these conditions, ion
25
26 migration would be expected to be easier at the NP/solution interface, consistent with our
27
28 observations of low E_{app} sensitivity for green-emitting sites. However, as mentioned above, we
29
30 do not observe size-dependant $I_{f\text{ red}}/I_{f\text{ green}}$ ratios to support the localization of green-emitting sites
31
32 near the surface.
33
34
35
36
37

38 CONCLUSIONS

39
40 In summary, we report a simple method for the formation of NPs of the conjugated
41
42 polyelectrolyte MPS-PPV that exhibit dim and red-shifted fluorescence. The chain conformation
43
44 of MPS-PPV is greatly influenced by the water content in H₂O/organic solvent mixtures and by
45
46 the choice of counterion. Tuning the solvent composition enables controlling the emission
47
48 intensity and color.
49
50
51

52
53 The newly prepared CPE NPs revealed heterogeneous fluorescence response to an externally
54
55 applied potential. The two-color SMS-EC setup used allowed us to spectrally discriminate
56
57
58
59
60

1
2
3 between deaggregated and aggregated emission sites. The deaggregated coiled MPS-PPV sites,
4 where ion rearrangement is less hindered, were less sensitive to changes in applied bias. We
5 postulate that the reduced sensitivity is a result of better compensation of the effects induced by
6 an applied potential due to higher electrolyte mobility. Quenching sites are present in the CPE,
7 most probably products of photooxidation of polymer segments, and are electrochemically
8 reducible in a reversible fashion which restores the fluorescence of the polymer. When migration
9 of ions through the NP is hindered, charge mobility between CPE segments is slowed down
10 leading to reduced electronic communication between chromophores in the NP and the working
11 electrode and affecting the repair of quenching sites.
12
13
14
15
16
17
18
19
20
21
22
23

24 Methods that influence CPE chain conformation are highly sought after to tune and improve
25 device applications, where a choice between either high charge mobility or high emission yield is
26 often necessary.²² Our two-color SMS-EC method herein described provides a tool to explore at
27 the single NP level the interplay between CPE conformation and its optoelectronic properties,
28 distinguishing between poorly and well-packed segments within single MPS-PPV NPs. Our
29 method thus enables evaluating the effectiveness of protocols that modify polymer chain
30 conformation either in solution or after deposition on a surface.
31
32
33
34
35
36
37
38
39
40
41
42

43 **Supporting Information Available:** Particle size distribution from SEM micrograph;
44 spectroscopic data for MPS-PPV NPs dispersed in H₂O/MeCN solutions; additional SMS-EC
45 data and representations; detailed mechanism of fluorescence enhancement under negative
46 applied biases. This material is available free of charge via the Internet at <http://pubs.acs.org>.
47
48
49
50
51
52

53 AUTHOR INFORMATION

54 **Corresponding Author**

1
2
3 *E-mail: gonzalo.cosa@mcgill.ca
4
5

6
7 **Notes**
8

9 The authors declare no competing financial interest.
10
11

12
13
14
15 **ACKNOWLEDGEMENTS**
16

17
18 G.C. is grateful to the Natural Science and Engineering Research Council of Canada (NSERC),
19 a Tomlinson award from McGill University, and the Canadian Foundation for Innovation (CFI)
20 for funding. R.G. is thankful to NSERC for a postgraduate scholarship. This work has been
21 supported in part by grants from the Agencia Nacional de Promoción Científica y Tecnológica
22 (ANPCyT), Argentina (PICT 140/08, 2213/07, 2691/11, and PRH23 PME01); the Consejo
23 Nacional de Investigaciones Científicas y Técnicas (CONICET), Argentina (PIP
24 11220090100839/10, 11220100100284/11, and CIAM/09); the Secretaría de Ciencia y Técnica,
25 UNRC Argentina; the Ministerio de Ciencia y Tecnología Córdoba, Argentina (PID 033/2010).
26
27 R.E.P. is permanent research staff of CONICET.
28
29
30
31
32
33
34
35
36
37
38
39
40
41
42
43
44
45
46
47
48
49
50
51
52
53
54
55
56
57
58
59
60

REFERENCES

1. Pinto, M. R.; Schanze, K. S., Conjugated Polyelectrolytes: Synthesis and Applications. *Synthesis* **2002**, *2002*, 1293-1309.
2. Burroughes, J. H.; Bradley, D. D. C.; Brown, A. R.; Marks, R. N.; Mackay, K.; Friend, R. H.; Burns, P. L.; Holmes, A. B., Light-Emitting Diodes Based on Conjugated Polymers. *Nature* **1990**, *347*, 539-541.
3. Günes, S.; Neugebauer, H.; Sariciftci, N. S., Conjugated Polymer-Based Organic Solar Cells. *Chem. Rev.* **2007**, *107*, 1324-1338.
4. Hoeben, F. J. M.; Jonkheijm, P.; Meijer, E. W.; Schenning, A. P. H. J., About Supramolecular Assemblies of π -Conjugated Systems. *Chem. Rev.* **2005**, *105*, 1491-1546.
5. Duarte, A.; Pu, K.-Y.; Liu, B.; Bazan, G. C., Recent Advances in Conjugated Polyelectrolytes for Emerging Optoelectronic Applications. *Chem. Mater.* **2010**, *23*, 501-515.
6. Chen, H.-Y.; Hou, J.; Zhang, S.; Liang, Y.; Yang, G.; Yang, Y.; Yu, L.; Wu, Y.; Li, G., Polymer Solar Cells with Enhanced Open-Circuit Voltage and Efficiency. *Nat. Photon.* **2009**, *3*, 649-653.
7. Ha, J. S.; Kim, K. H.; Choi, D. H., 2,5-bis(2-octyldodecyl)pyrrolo[3,4-C]pyrrole-1,4-(2H,5H)-dione-Based Donor–Acceptor Alternating Copolymer Bearing 5,5'-di(thiophen-2-yl)-2,2'-biselenophene Exhibiting $1.5 \text{ Cm}^2 \cdot \text{V}^{-1} \cdot \text{S}^{-1}$ Hole Mobility in Thin-Film Transistors. *J. Am. Chem. Soc.* **2011**, *133*, 10364-10367.

- 1
2
3 8. Thomas, S. W.; Joly, G. D.; Swager, T. M., Chemical Sensors Based on Amplifying
4
5
6
7
8
9
10
11
12
13
14
15
16
17
18
19
20
21
22
23
24
25
26
27
28
29
30
31
32
33
34
35
36
37
38
39
40
41
42
43
44
45
46
47
48
49
50
51
52
53
54
55
56
57
58
59
60
Fluorescent Conjugated Polymers. *Chem. Rev.* **2007**, *107*, 1339-1386.
9. Hu, D.; Yu, J.; Wong, K.; Bagchi, B.; Rossky, P. J.; Barbara, P. F., Collapse of Stiff
Conjugated Polymers with Chemical Defects into Ordered, Cylindrical Conformations. *Nature*
2000, *405*, 1030-1033.
10. Kim, J.; Swager, T. M., Control of Conformational and Interpolymer Effects in
Conjugated Polymers. *Nature* **2001**, *411*, 1030-1034.
11. Sarzi Sartori, S.; De Feyter, S.; Hofkens, J.; Van der Auweraer, M.; De Schryver, F.;
Brunner, K.; Hofstraat, J. W., Host Matrix Dependence on the Photophysical Properties of
Individual Conjugated Polymer Chains. *Macromolecules* **2003**, *36*, 500-507.
12. Ebihara, Y.; Vacha, M., Relating Conformation and Photophysics in Single MEH-PPV
Chains. *J. Phys. Chem. B* **2008**, *112*, 12575-12578.
13. Lupton, J. M., Chromophores in Conjugated Polymers—All Straight? *ChemPhysChem*
2012, *13*, 901-907.
14. Botiz, I.; Stingelin, N., Influence of Molecular Conformations and Microstructure on the
Optoelectronic Properties of Conjugated Polymers. *Materials* **2014**, *7*, 2273-2300.
15. Nguyen, T.-Q.; Martini, I. B.; Liu, J.; Schwartz, B. J., Controlling Interchain Interactions
in Conjugated Polymers: The Effects of Chain Morphology on Exciton–Exciton Annihilation
and Aggregation in MEH-PPV Films. *J. Phys. Chem. B* **2000**, *104*, 237-255.

- 1
2
3 16. Kobayashi, H.; Hirata, S.; Vacha, M., Mechanical Manipulation of Photophysical
4 Properties of Single Conjugated Polymer Nanoparticles. *J. Phys. Chem. Lett.* **2013**, *4*, 2591-
5 2596.
6
7
8
9
10
11 17. Woll, D.; Braeken, E.; Deres, A.; De Schryver, F. C.; Uji-i, H.; Hofkens, J., Polymers and
12 Single Molecule Fluorescence Spectroscopy, What Can We Learn? *Chem. Soc. Rev.* **2009**, *38*,
13 313-328.
14
15
16
17
18
19 18. Schwartz, B. J., Conjugated Polymers as Molecular Materials: How Chain Conformation
20 and Film Morphology Influence Energy Transfer and Interchain Interactions. *Annu. Rev. Phys.*
21 *Chem.* **2003**, *54*, 141-172.
22
23
24
25
26
27 19. Nguyen, T.-Q.; Wu, J.; Doan, V.; Schwartz, B. J.; Tolbert, S. H., Control of Energy
28 Transfer in Oriented Conjugated Polymer-Mesoporous Silica Composites. *Science* **2000**, *288*,
29 652-656.
30
31
32
33
34
35 20. Hu, Z.; Adachi, T.; Haws, R.; Shuang, B.; Ono, R. J.; Bielawski, C. W.; Landes, C. F.;
36 Rosky, P. J.; Vanden Bout, D. A., Excitonic Energy Migration in Conjugated Polymers: The
37 Critical Role of Interchain Morphology. *J. Am. Chem. Soc.* **2014**.
38
39
40
41
42
43 21. Hwang, I.; Scholes, G. D., Electronic Energy Transfer and Quantum-Coherence in π -
44 Conjugated Polymers. *Chem. Mater.* **2011**, *23*, 610-620.
45
46
47
48
49 22. Garcia, A.; Nguyen, T.-Q., Effect of Aggregation on the Optical and Charge Transport
50 Properties of an Anionic Conjugated Polyelectrolyte. *J. Phys. Chem. C* **2008**, *112*, 7054-7061.
51
52
53
54
55
56
57
58
59
60

- 1
2
3 23. Wang, D.; Lal, J.; Moses, D.; Bazan, G. C.; Heeger, A. J., Small Angle Neutron
4 Scattering (SANS) Studies of a Conjugated Polyelectrolyte in Aqueous Solution. *Chem. Phys.*
5
6 *Lett.* **2001**, *348*, 411-415.
7
8
9
10
11 24. Gao, Y.; Wang, C.-C.; Wang, L.; Wang, H.-L., Conjugated Polyelectrolytes with Ph-
12
13 Dependent Conformations and Optical Properties. *Langmuir* **2007**, *23*, 7760-7767.
14
15
16
17 25. Schnablegger, H.; Antonietti, M.; Göltner, C.; Hartmann, J.; Cölfen, H.; Samori, P.;
18
19 Rabe, J. P.; Häger, H.; Heitz, W., Morphological Characterization of the Molecular
20
21 Superstructure of Polyphenylene Ethynylene Derivatives. *J. Colloid Interface Sci.* **1999**, *212*, 24-
22
23 32.
24
25
26
27 26. Palacios, R. E.; Fan, F.-R. F.; Grey, J. K.; Suk, J.; Bard, A. J.; Barbara, P. F., Charging
28
29 and Discharging of Single Conjugated-Polymer Nanoparticles. *Nat Mater* **2007**, *6*, 680-685.
30
31
32
33 27. Szymanski, C.; Wu, C.; Hooper, J.; Salazar, M. A.; Perdomo, A.; Dukes, A.; McNeill, J.,
34
35 Single Molecule Nanoparticles of the Conjugated Polymer MEH-PPV, Preparation and
36
37 Characterization by near-Field Scanning Optical Microscopy. *J. Phys. Chem. B* **2005**, *109*, 8543-
38
39 8546.
40
41
42
43 28. Tuncel, D.; Demir, H. V., Conjugated Polymer Nanoparticles. *Nanoscale* **2010**, *2*, 484-
44
45 494.
46
47
48
49 29. Pecher, J.; Mecking, S., Nanoparticles of Conjugated Polymers. *Chem. Rev.* **2010**, *110*,
50
51 6260-6279.
52
53
54
55 30. Wu, C.; Chiu, D. T., Highly Fluorescent Semiconducting Polymer Dots for Biology and
56
57 Medicine. *Angew. Chem. Int. Ed.* **2013**, *52*, 3086-3109.
58
59
60

- 1
2
3 31. Bustamante, C.; Maestre, M. F., Statistical Effects in the Absorption and Optical Activity
4 of Particulate Suspensions. *Proc. Natl. Acad. Sci. U. S. A.* **1988**, *85*, 8482-8486.
5
6
7
8
9 32. Choi, J.; Ruiz, C. R.; Nesterov, E. E., Temperature-Induced Control of Conformation and
10 Conjugation Length in Water-Soluble Fluorescent Polythiophenes. *Macromolecules* **2010**, *43*,
11 1964-1974.
12
13
14
15
16
17 33. Tretiak, S.; Saxena, A.; Martin, R. L.; Bishop, A. R., Interchain Electronic Excitations in
18 Poly(phenylenevinylene) (PPV) Aggregates. *J. Phys. Chem. B* **2000**, *104*, 7029-7037.
19
20
21
22
23 34. Pinto, M. R.; Kristal, B. M.; Schanze, K. S., A Water-Soluble Poly(phenylene
24 Ethynylene) with Pendant Phosphonate Groups. Synthesis, Photophysics, and Layer-by-Layer
25 Self-Assembled Films. *Langmuir* **2003**, *19*, 6523-6533.
26
27
28
29
30 35. Traiphol, R.; Charoenthai, N.; Srihirin, T.; Kerdcharoen, T.; Osotchan, T.; Maturros, T.,
31 Chain Organization and Photophysics of Conjugated Polymer in Poor Solvents: Aggregates,
32 Agglomerates and Collapsed Coils. *Polymer* **2007**, *48*, 813-826.
33
34
35
36
37
38 36. Wang, M.; Zou, S.; Guerin, G.; Shen, L.; Deng, K.; Jones, M.; Walker, G. C.; Scholes, G.
39 D.; Winnik, M. A., A Water-Soluble Ph-Responsive Molecular Brush of Poly(N,N-
40 dimethylaminoethyl Methacrylate) Grafted Polythiophene. *Macromolecules* **2008**, *41*, 6993-
41 7002.
42
43
44
45
46
47
48 37. Feist, F. A.; Zickler, M. F.; Basché, T., Origin of the Red Sites and Energy Transfer
49 Rates in Single MEH-PPV Chains at Low Temperature. *ChemPhysChem* **2011**, *12*, 1499-1508.
50
51
52
53
54
55
56
57
58
59
60

1
2
3
4
5
6
7
8
9
10
11
12
13
14
15
16
17
18
19
20
21
22
23
24
25
26
27
28
29
30
31
32
33
34
35
36
37
38
39
40
41
42
43
44
45
46
47
48
49
50
51
52
53
54
55
56
57
58
59
60

38. Potai, R.; Traiphol, R., Controlling Chain Organization and Photophysical Properties of Conjugated Polymer Nanoparticles Prepared by Reprecipitation Method: The Effect of Initial Solvent. *J. Colloid Interface Sci.* **2013**, *403*, 58-66.

39. Lemmer, U.; Heun, S.; Mahrt, R. F.; Scherf, U.; Hopmeier, M.; Siegner, U.; Göbel, E. O.; Müllen, K.; Bässler, H., Aggregate Fluorescence in Conjugated Polymers. *Chem. Phys. Lett.* **1995**, *240*, 373-378.

40. Aryanpour, K.; Sheng, C. X.; Olejnik, E.; Pandit, B.; Psiachos, D.; Mazumdar, S.; Vardeny, Z. V., Evidence for Excimer Photoexcitations in an Ordered π -Conjugated Polymer Film. *Phys. Rev. B* **2011**, *83*, 155124.

41. Smith, A.; Shen, C.-F.; Roberts, S.; Helgeson, R.; Schwartz, B., Ionic Strength and Solvent Control over the Physical Structure, Electronic Properties and Superquenching of Conjugated Polyelectrolytes. *Res. Chem. Intermed.* **2007**, *33*, 125-142.

42. Jakubiak, R.; Collison, C. J.; Wan, W. C.; Rothberg, L. J.; Hsieh, B. R., Aggregation Quenching of Luminescence in Electroluminescent Conjugated Polymers. *J. Phys. Chem. A* **1999**, *103*, 2394-2398.

43. Collini, E.; Scholes, G. D., Coherent Intrachain Energy Migration in a Conjugated Polymer at Room Temperature. *Science* **2009**, *323*, 369-373.

44. Hoven, C. V.; Garcia, A.; Bazan, G. C.; Nguyen, T.-Q., Recent Applications of Conjugated Polyelectrolytes in Optoelectronic Devices. *Adv. Mater.* **2008**, *20*, 3793-3810.

45. Yang, R.; Garcia, A.; Korystov, D.; Mikhailovsky, A.; Bazan, G. C.; Nguyen, T.-Q., Control of Interchain Contacts, Solid-State Fluorescence Quantum Yield, and Charge Transport

1
2
3 of Cationic Conjugated Polyelectrolytes by Choice of Anion. *J. Am. Chem. Soc.* **2006**, *128*,
4
5 16532-16539.
6
7

8
9 46. Palacios, R. E.; Fan, F.-R. F.; Bard, A. J.; Barbara, P. F., Single-Molecule
10 Spectroelectrochemistry (SMS-EC). *J. Am. Chem. Soc.* **2006**, *128*, 9028-9029.
11
12

13
14 47. Bard, A. J.; Faulkner, L. R., *Electrochemical Methods: Fundamentals and Applications*.
15
16 2nd ed.; Wiley: Hoboken, 2001.
17
18

19
20 48. Palacios, R. E.; Chang, W.-S.; Grey, J. K.; Chang, Y.-L.; Miller, W. L.; Lu, C.-Y.;
21
22 Henkelman, G.; Zepeda, D.; Ferraris, J.; Barbara, P. F., Detailed Single-Molecule
23 Spectroelectrochemical Studies of the Oxidation of Conjugated Polymers. *J. Phys. Chem. B*
24
25 **2009**, *113*, 14619-14628.
26
27

28
29
30 49. Li, Y.; Cao, Y.; Gao, J.; Wang, D.; Yu, G.; Heeger, A. J., Electrochemical Properties of
31
32 Luminescent Polymers and Polymer Light-Emitting Electrochemical Cells. *Synth. Met.* **1999**, *99*,
33
34 243-248.
35
36

37
38 50. Holt, A. L.; Leger, J. M.; Carter, S. A., Electrochemical and Optical Characterization of
39
40 P- and N-Doped Poly[2-methoxy-5-(2-ethylhexyloxy)-1,4-phenylenevinylene]. *J. Chem. Phys.*
41
42 **2005**, *123*, 044704 1-7.
43
44

45
46 51. Deussen, M.; Scheidler, M.; Bäessler, H., Electric Field-Induced Photoluminescence
47
48 Quenching in Thin-Film Light-Emitting Diodes Based on Poly(phenyl-p-phenylene Vinylene).
49
50 *Synth. Met.* **1995**, *73*, 123-129.
51
52

1
2
3
4
5
6
7
8
9
10
11
12
13
14
15
16
17
18
19
20
21
22
23
24
25
26
27
28
29
30
31
32
33
34
35
36
37
38
39
40
41
42
43
44
45
46
47
48
49
50
51
52
53
54
55
56
57
58
59
60

52. Smith, T. M.; Hazelton, N.; Peteanu, L. A.; Wildeman, J., Electrofluorescence of MEH-PPV and Its Oligomers: Evidence for Field-Induced Fluorescence Quenching of Single Chains. *J. Phys. Chem. B* **2006**, *110*, 7732-7742.

53. Moscatelli, A.; Livingston, K.; So, W. Y.; Lee, S. J.; Scherf, U.; Wildeman, J.; Peteanu, L. A., Electric-Field-Induced Fluorescence Quenching in Polyfluorene, Ladder-Type Polymers, and MEH-PPV: Evidence for Field Effects on Internal Conversion Rates in the Low Concentration Limit. *J. Phys. Chem. B* **2010**, *114*, 14430-14439.

54. Heinze, J.; Tschuncky, P., Electrochemical Properties. In *Electronic Materials: The Oligomer Approach*, Wiley-VCH Verlag GmbH: 1998; pp 479-514.

55. Wu, H.; Huang, F.; Mo, Y.; Yang, W.; Wang, D.; Peng, J.; Cao, Y., Efficient Electron Injection from a Bilayer Cathode Consisting of Aluminum and Alcohol-/Water-Soluble Conjugated Polymers. *Adv. Mater.* **2004**, *16*, 1826-1830.

56. Wu, H.; Huang, F.; Peng, J.; Cao, Y., High-Efficiency Electron Injection Cathode of Au for Polymer Light-Emitting Devices. *Org. Electron.* **2005**, *6*, 118-128.

57. Ishii, H.; Sugiyama, K.; Ito, E.; Seki, K., Energy Level Alignment and Interfacial Electronic Structures at Organic/Metal and Organic/Organic Interfaces. *Adv. Mater.* **1999**, *11*, 605-625.

58. Hoven, C. V.; Peet, J.; Mikhailovsky, A.; Nguyen, T.-Q., Direct Measurement of Electric Field Screening in Light Emitting Diodes with Conjugated Polyelectrolyte Electron Injecting/Transport Layers. *Appl. Phys. Lett.* **2009**, *94*, 033301 1-3.

1
2
3 59. Nguyen, T.-Q.; Schwartz, B. J.; Schaller, R. D.; Johnson, J. C.; Lee, L. F.; Haber, L. H.;
4 Saykally, R. J., Near-Field Scanning Optical Microscopy (NSOM) Studies of the Relationship
5 between Interchain Interactions, Morphology, Photodamage, and Energy Transport in
6 Conjugated Polymer Films. *J. Phys. Chem. B* **2001**, *105*, 5153-5160.
7

8
9
10
11
12
13 60. Schaller, R. D.; Snee, P. T.; Johnson, J. C.; Lee, L. F.; Wilson, K. R.; Haber, L. H.;
14 Saykally, R. J.; Nguyen, T.-Q.; Schwartz, B. J., Nanoscopic Interchain Aggregate Domain
15 Formation in Conjugated Polymer Films Studied by Third Harmonic Generation near-Field
16 Scanning Optical Microscopy. *J. Chem. Phys.* **2002**, *117*, 6688-6698.
17
18
19
20
21
22

23
24 61. Nguyen, T. Q.; Wu, J.; Tolbert, S. H.; Schwartz, B. J., Control of Energy Transport in
25 Conjugated Polymers Using an Ordered Mesoporous Silica Matrix. *Adv. Mater.* **2001**, *13*, 609-
26
27
28
29
30
31
32
33
34
35
36
37
38
39
40
41
42
43
44
45
46
47
48
49
50
51
52
53
54
55
56
57
58
59
60

62. Heeger, A. J.; Kivelson, S.; Schrieffer, J. R.; Su, W. P., Solitons in Conducting Polymers.
Rev. Mod. Phys. **1988**, *60*, 781-850.

63. Garcia, A.; Bakus Ii, R. C.; Zalar, P.; Hoven, C. V.; Brzezinski, J. Z.; Nguyen, T.-Q.,
Controlling Ion Motion in Polymer Light-Emitting Diodes Containing Conjugated
Polyelectrolyte Electron Injection Layers. *J. Am. Chem. Soc.* **2011**, *133*, 2492-2498.

64. Liu, H.-W.; Ngo, A. T.; Cosa, G., Enhancing the Emissive Properties of Poly(p-
phenylenevinylene)-Conjugated Polyelectrolyte-Coated SiO₂ Nanoparticles. *J. Am. Chem. Soc.*
2011, *134*, 1648-1652.

65. Park, S.-J.; Gesquiere, A. J.; Yu, J.; Barbara, P. F., Charge Injection and Photooxidation
of Single Conjugated Polymer Molecules. *J. Am. Chem. Soc.* **2004**, *126*, 4116-4117.

1
2
3 66. Gesquiere, A. J.; Park, S.-J.; Barbara, P. F., F–V/SMS: A New Technique for Studying
4 the Structure and Dynamics of Single Molecules and Nanoparticles. *J. Phys. Chem. B* **2004**, *108*,
5 10301-10308.
6
7

8
9
10
11 67. Cornil, J.; dos Santos, D. A.; Crispin, X.; Silbey, R.; Brédas, J. L., Influence of Interchain
12 Interactions on the Absorption and Luminescence of Conjugated Oligomers and Polymers: A
13 Quantum-Chemical Characterization. *J. Am. Chem. Soc.* **1998**, *120*, 1289-1299.
14
15

16
17
18
19 68. Stringle, D. L. B.; Nevin Campbell, R.; Workentin, M. S., Radical Anion Chain Process
20 Initiated by a Dissociative Electron Transfer to a Monocyclic Endoperoxide. *Chem. Commun.*
21 **2003**, 1246-1247.
22
23

24
25
26
27 69. Scurlock, R. D.; Wang, B.; Ogilby, P. R.; Sheats, J. R.; Clough, R. L., Singlet Oxygen as
28 a Reactive Intermediate in the Photodegradation of an Electroluminescent Polymer. *J. Am.*
29 *Chem. Soc.* **1995**, *117*, 10194-10202.
30
31

32
33
34
35 70. Dam, N.; Scurlock, R. D.; Wang, B.; Ma, L.; Sundahl, M.; Ogilby, P. R., Singlet Oxygen
36 as a Reactive Intermediate in the Photodegradation of Phenylenevinylene Oligomers. *Chem.*
37 *Mater.* **1999**, *11*, 1302-1305.
38
39

40
41
42
43 71. Burrows, H. D.; Narwark, O.; Peetz, R.; Thorn-Csanyi, E.; Monkman, A. P.; Hamblett, I.;
44 Navaratnam, S., Mechanistic Studies on the Photodegradation of 2,5-Dialkyloxy-Substituted
45 Para-Phenylenevinylene Oligomers by Singlet Oxygen. *Photochem. Photobio. Sci.* **2010**, *9*, 942-
46 948.
47
48
49
50
51

1
2
3 72. Chambon, S.; Rivaton, A.; Gardette, J.-L.; Firon, M., Photo- and Thermo-Oxidation of
4 Poly(p-phenylene-vinylene) and Phenylene-Vinylene Oligomer. *Polym. Degrad. Stab.* **2011**, *96*,
5 1149-1158.
6
7

8
9
10
11 73. Guerlin, A.; Dumur, F.; Dumas, E.; Miomandre, F.; Wantz, G.; Mayer, C. R., Tunable
12 Optical Properties of Chromophores Derived from Oligo(p-phenylene Vinylene). *Org. Lett.*
13 **2010**, *12*, 2382-2385.
14
15

16
17
18
19 74. Silvester, D. S.; He, W.; Aldous, L.; Hardacre, C.; Compton, R. G., Electrochemical
20 Reduction of Benzoic Acid and Substituted Benzoic Acids in Some Room Temperature Ionic
21 Liquids. *J. Phys. Chem. C* **2008**, *112*, 12966-12973.
22
23

24
25
26
27 75. Bolinger, J. C.; Fradkin, L.; Lee, K.-J.; Palacios, R. E.; Barbara, P. F., Light-Assisted
28 Deep-Trapping of Holes in Conjugated Polymers. *Proc. Natl. Acad. Sci. U. S. A.* **2009**, *106*,
29 1342-1346.
30
31

32
33
34
35 76. Grey, J. K.; Kim, D. Y.; Norris, B. C.; Miller, W. L.; Barbara, P. F., Size-Dependent
36 Spectroscopic Properties of Conjugated Polymer Nanoparticles. *J. Phys. Chem. B* **2006**, *110*,
37 25568-25572.
38
39

40
41
42
43 77. Peteanu, L. A.; Sherwood, G. A.; Werner, J. H.; Shreve, A. P.; Smith, T. M.; Wildeman,
44 J., Visualizing Core-Shell Structure in Substituted Ppv Oligomer Aggregates Using
45 Fluorescence Lifetime Imaging Microscopy (FLIM). *J. Phys. Chem. C* **2011**, *115*, 15607-15616.
46
47

48
49
50
51 78. So, W. Y.; Hong, J.; Kim, J. J.; Sherwood, G. A.; Chacon-Madrid, K.; Werner, J. H.;
52 Shreve, A. P.; Peteanu, L. A.; Wildeman, J., Effects of Solvent Properties on the Spectroscopy
53
54

1
2
3 and Dynamics of Alkoxy-Substituted PPV Oligomer Aggregates. *J. Phys. Chem. B* **2012**, *116*,
4
5 10504-10513.
6
7
8
9
10
11
12
13
14
15
16
17
18
19
20
21
22
23
24
25
26
27
28
29
30
31
32
33
34
35
36
37
38
39
40
41
42
43
44
45
46
47
48
49
50
51
52
53
54
55
56
57
58
59
60

1
2
3 For Table of Contents Only
4
5
6
7
8
9
10
11
12
13
14
15
16
17
18
19
20
21
22
23
24
25
26
27
28
29
30
31
32
33
34
35
36
37
38
39
40
41
42
43
44
45
46
47
48
49
50
51
52
53
54
55
56
57
58
59
60

